ORIGINAL ARTICLE

Effect of particle size on thermomechanical properties of particulate polymer composite

M. Hossein Alaei · Puneet Mahajan ·
Mathias Brieu · Djimedo Kondo · S. Javed Ahmed Rizvi ·
Sandeep Kumar · Naresh Bhatnagar

Abstract Particulate composite materials (PCM) consisting of a matrix reinforced by micro to nano-sized dispersed phase are receiving the attention of designers as a promising futuristic materials. This study unearths the thermal and mechanical behavior of maleic anhydride grafted polypropylene/silica (MA-g-PP/silica) composites for reinforcement ranging from micro- to nano-size. The monodisperse silica spherical particles were used in all the formulations of composites. Further the volume fraction was kept the same in all the compounded thermoplastic composites ranging from 100 nm to 130 μm in a co-rotating conical twin-screw micro-compounder. The micrographs were obtained from transmission electron microscopy (TEM) and the scanning electron microscopy (SEM). The SEM and TEM results revealed a good dispersion of the silica spheres within the MA-g-PP matrix. The compounded composite materials were injection molded to fabricate tensile test specimens (ASTM D638 type V) and tested for tensile properties. In order to investigate the effect of particle size on crystallite structure of the matrix, the composites were tested on differential scanning calorimeter and X-ray diffraction (WAXD). The thermal stability and degradation kinetics were studied via thermogravimetric analysis. The results show increase in crystallization rate, crystallinity percentage, Young's modulus, strength and thermal stability of MA-g-PP by addition of the silica particles. Further it was observed that the small-sized dispersed phase had better overall thermal and mechanical behavior than its larger sized counterpart.

Keywords Silica sphere · DSC · TGA · XRD · DIC

M. H. Alaei (✉) · P. Mahajan
Department of Applied Mechanics, Indian Institute
of Technology, Delhi, New Delhi 110016, India
e-mail: mallaee@yahoo.com

M. Brieu
Institut Jean le Rond d'Alembert Université Pierre et Marie
Curie (UPMC), Paris, France

D. Kondo
Laboratoire de Mecanique de Lille-UMR 8107, École Centrale
de Lille, Villeneuve-d'Ascq, France

S. J. A. Rizvi · N. Bhatnagar
Department of Mechanical Engineering, Indian Institute
of Technology, Delhi, New Delhi 110016, India

S. Kumar
Centers for Polymer Science and Engineering, Indian Institute
of Technology, Delhi, New Delhi 110016, India

Introduction

Particulate composites are materials which consist of, or include particles that combine more than one physical phase in a controlled fashion. These materials have the potential to enable some of its properties and property combinations to unprecedented extremes. Within the parameters affecting the final properties of particulate composites, particle size is known to be among the main factors [1–3]. It is reported in the literature that the addition of filler particles to a matrix could improve mechanical and thermal properties [4–6].

The thermo-physical properties of a composite are highly affected by the change in reinforcement size of a composite [7, 8]. Nanofillers can markedly improve the thermal, electrical, and mechanical properties of a polymer composite, such as the strength, modulus, and dimensional stability, as compared with microfillers [9–11]. However, unlike microfillers that usually cause the glass transition temperature (T_g) of a polymer to increase [12–14], the effect of nanofillers on the T_g of the polymer matrix is found to be inconsistent.

Although the T_g of the polymer can be increased by nanofillers as shown in some cases [15–17], T_g decreases [18–20] with no obvious change in T_g [21], and an initial increase in T_g followed by a decrease in T_g with a higher nanofiller content has also been reported [22]; which indicates difference of opinions and that no consistent perception exists at this moment. As T_g is a very important property in determination of a polymer suitability for engineering applications, the difference in changes between T_g's caused by either microfillers or nanofillers is worthy of deep investigation.

The present study reveals that the drastic improvement in mechanical properties of MA-g-PP matrix is possible by the incorporation of monodisperse spherical-silica particles ranging from micro- to nano-scale sizes [23, 24]. Stiffness of polymer composites can be readily improved by the addition of micro- to nanoparticles since their stiffness is normally superior to the stiffness of the polymer matrix [25–27]. Particle size has an obvious effect on these mechanical properties. For example, smaller calcium carbonate particles provide higher strength of filled polypropylene composites at a given particle loading [28]. However, strength strongly depends on the stress transfer between the particles and the matrix. For example, the tensile strength of glass bead filled polystyrene composites depends on the particle–matrix adhesion and increases with it [25].

As revealed from the above literature, elaborative research has been carried out on the aforementioned topics but joint studies on the effect of particle size on the thermal and mechanical properties together are not yet fully available. Most of the investigations have been focused on the effect of particle size on either the thermal or mechanical properties of composites in which size effect might be (in very few cases) or might not be the only variable, i.e., there is a combination of variables like material of both particle and matrix, processing parameters, shape and size of particles, etc. The results of these investigations show the combined effect of particle size and reinforcing parameters on the overall properties [6]. Therefore, it is difficult to understand the effect of size alone on the thermomechanical properties of composites. This research study is focused solely to understand the variation that occurs at various thermal stages due to the change in particle size only by keeping all other parameters constant (material of matrix and particles, shape, processing parameters, etc.) that would later affect the mechanical properties of these composites.

Experimental

Materials

The silica micro- and nanospheres (sphericity ∼1.0) from XL Sci-Tech, USA, in sizes of 100, 250, 750 nm and 4, 70 and 130 μm were used as reinforcement for MA-g-PP matrix. Figure 1 shows SEM microphotograph of 130 μm, 70 μm, 4 μm and 750 nm silica powders. Polypropylene (PP) grafted maleic anhydride (MA-g-PP) and acid functionality with the trade name of OPTIM® P-406 obtained from M/s. Pluss Polymers, India were used as the matrix for the composite. The MFR of polymer was measured to be 40 g/10 min (2.16 kg, 190 °C). The bulk density of polymer was 0.91 g/cc and crystalline melting point was found to be 154.7 °C by DSC.

An equal volume fraction of 0.03 of particle reinforcement was selected for all the MA-g-PP/silica composites to see its size effect. In the dry blending, the calculated amounts of MA-g-PP and silica sphere particles were mixed together in a manual tumbler and then dried for 8 h in a vacuum oven at 70 °C temperature and 50 mmHg vacuum to remove moisture before feeding to the compounder. Composite compositions are summarized in Table 1.

Melt compounding

A co-rotating conical twin-screw micro-compounder (with internal melt recirculation for batch processing), from M/s. DSM Research, The Netherlands, model 5 mL, was used for the compounding of various compositions of MA-g-PP/silica composites at the screw RPM of 130 and barrel temperature of 190 °C for 10 min under nitrogen atmosphere.

Injection molding

The tensile test specimens (ASTM 638, type-5) were molded by microinjection molding system of M/s, Thermo Electron Corp., Germany, Model Haake MiniJet. The processing parameters were as follows:

Melt temperature	200 °C
Injection pressure	700 bar
Packing pressure	350 bar
Cooling time	12 s

Characterization of composites

Among the various techniques of morphological characterization of the polymer composite, transmission electron microscopy (TEM) and scanning electron microscopy (SEM) have been used. The samples for TEM were microtomed using ultramicrotome (Leica, USA), having 100 nm thickness, stained with uranyl acetate for 15 min and lead citrate for 5 min and fixed onto a copper grid of 3.05 mm. The samples were scanned on TEM (Jeol, Japan, model-2100F). The TEM micrograph, at 200 kV, of MS 100 nm is shown in Fig. 2. The samples were cryogenically fractured in liquid nitrogen for SEM study, then gold
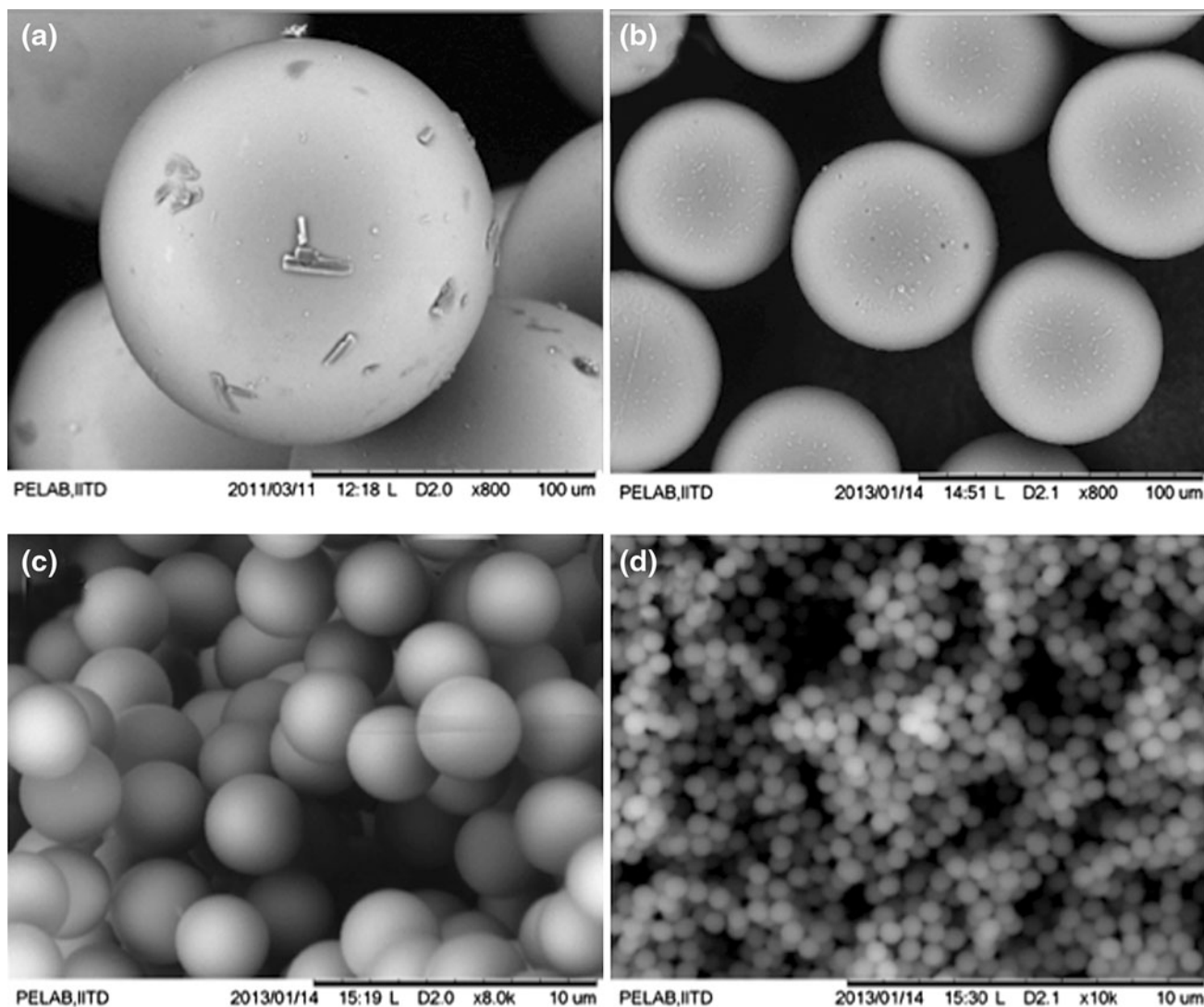
Fig. 1 SEM microphotographs of **a** 130 μm, **b** 70 μm, **c** 4 μm and **d** 750 nm silica powder

Table 1 Composition of the composites

Designation	Composite composition		
	Matrix	Particle volume fraction (%)	Particle size
MA-g-PP	MA-g-PP	0	–
MS 130μ	MA-g-PP	3	130 μm
MS 70μ	MA-g-PP	3	70 μm
MS 4μ	MA-g-PP	3	4 μm
MS 750 nm	MA-g-PP	3	750 nm
MS 250 nm	MA-g-PP	3	250 nm
MS 100 nm	MA-g-PP	3	100 nm

coated and analyzed using scanning electron microscope (Carl Zeiss AG, model: EVO® 50 Series). The SEM micrographs are shown in Fig. 3. It can be observed that a

good dispersion of silica particles has been achieved within the MA-g-PP matrix.

Thermal characterization

Differential scanning calorimetry (DSC)

The DSC was used to investigate the crystallization and melting behavior of the prepared composites. The DSC scans were recorded using a Perkin Elmer Pyris 7 calorimeter. Bits of test samples, weighing 6 ± 2 mg, were heated to 180 °C at a rate of 20 °C/min and kept for 3 min to remove the thermal history. Afterward, the samples were cooled down to 40 °C at a cooling rate of 10 °C/min, and heated again to 180 °C at the rate of 10 °C/min. This experiment was performed for each sample of composite. The second heating scans were used to study the crystallization since first heating

was done to remove the thermal history from the material. The exothermic and endothermic peaks were termed as crystallization temperature (T_{exo}) and melting endothermic temperature, T_m. The area of crystallization and melting peaks are used to calculate the crystallization enthalpy (ΔH_c)

Fig. 2 TEM microphotograph of MS 100 nm at 200 kV

and the heat of fusion (ΔH_f), respectively. The summary of the cooling and the heating scans for DSC can be observed in Tables 2 and 3, respectively. The maximum temperature limits for the heating scan were chosen based on the melting range of the following equation [29];

$$X_c = \left(\frac{\Delta H_f}{\Delta H_{100\,w}} \right) \times 100 \tag{1}$$

Where ΔH_f is the heat of fusion, ΔH_{100} is the heat of fusion for 100 % crystalline PP (ΔH_{100} of MA-g-PP was not available) and w is the mass fraction for matrix in the composites. The heat of fusion of 100 % crystalline PP is taken as 207 J/g [30].

Thermogravimetric analysis (TGA)

Thermal stability of MA-g-PP/silica composites (particles size ranging from micro- to nanometer levels) was determined by recording TG/DTG traces in an inert (nitrogen) atmosphere. Perkin Elmer Pyris 6 having TG module was used for this purpose. The dynamic scans were run from
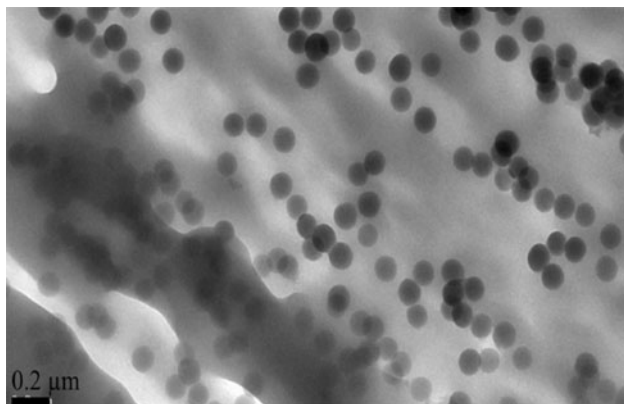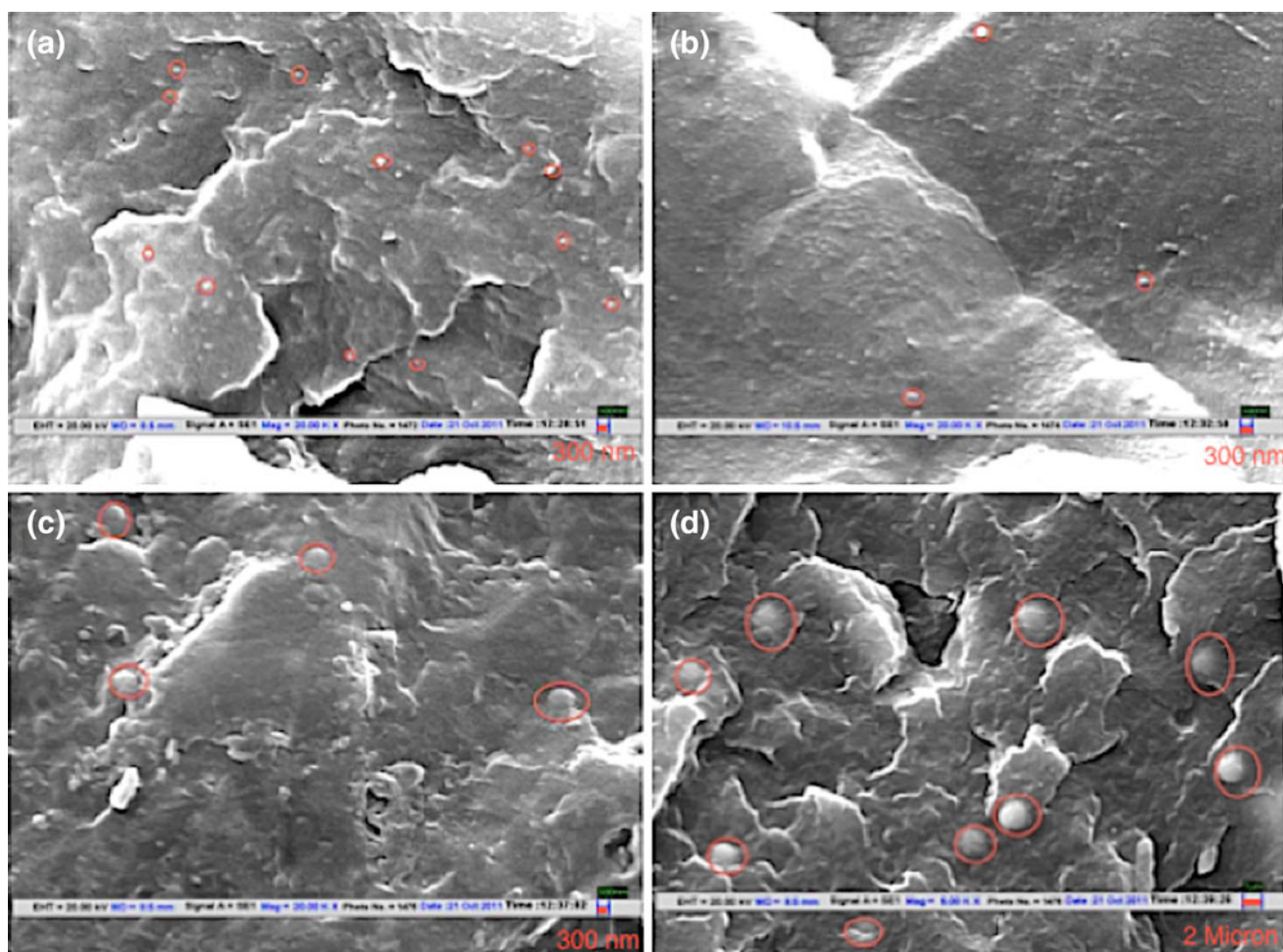

Fig. 3 SEM micrographs of **a** MS 100 nm, **b** MS 250 nm, **c** MS 750 nm and **d** MS 4μ showing the dispersion of the spherical particles

Table 2 Results of cooling scans recorded from the DSC graph

Material	T_{exo}	T_s	ΔH_c (J/g)	$T_s - T_{exo}$	$S_{i (tan \alpha)}$
MA-g-PP	114.88	118.27	92.251	3.39	78 (4.7)
MS 130μ	115.33	119.47	98.15	4.14	85.2 (11.9)
MS 70μ	116.1	120.33	99.44	4.23	86.1 (14.66)
MS 4μ	116.33	120.7	101.8	4.37	86.31 (15.5)
MS 750 nm	116.44	120.82	104.5	4.38	86.6 (16.8)
MS 250 nm	118.5	122.98	103.3	4.48	86.8 (17.8)
MS 100 nm	119.1	125.04	108.8	5.94	86.9 (18.34)

Table 3 DSC melting scans data of composites

Material	T_m	T_{om}	ΔH_f (J/g)
MA-g-PP	157.74	152.85	63.833
MS 130μ	159.38	153.94	99.43
MS 70μ	159.36	153.67	101.6
MS 4μ	159.84	153.62	102.2
MS 750 nm	159.91	153.81	104
MS 250 nm	160.06	153.34	106.7
MS 100 nm	160.63	154.11	106.2

room temperature to 700 °C at a heating rate of 20 °C/min. The average weight of tested TGA samples used in each experiment was 9 ± 2 mg. It is already defined in the literature that the residual weight measured during the TGA test can be converted to the corresponding value of percentage of the residual weight fraction, $[w_r(\%) = 100 * (w_t/w_0)]$, where w_t is the mass of the sample at each temperature and w_0 is the initial mass of the sample. The derivative curves (DTG) were obtained to compare the weight loss rate in the entire range of the temperature. The temperature at which the slope of the weight vs. temperature curve starts to decrease was noted as the temperature of the degradation initiation (TDI) [7]. The TGA and DTG thermographs of the composite samples are shown in Fig. 4. Thermal degradation parameters of TGA are summarized in Table 4.

Wide angle X-ray scattering (WAXS)

X-ray diffractograms [scan range $(2\theta) = 10°–80°$, scan speed: $2.0° min^{-1}$] of the composite samples were obtained with a PANalytical X-ray diffractometer having an X-ray tube producing monochromatic Cu-Kα radiation. The MA-g-PP and composite sheets were mounted onto sample stage to record the diffraction patterns and crystallinity index. The sample stage was mounted on horizontal axis and the diffracted beam optics and the detector was mounted onto 2θ axis. The diffractograms are shown in Fig. 5. D spacing and peak intensity obtained from XRD diffractograms are shown in Tables 5 and 6, respectively.

The crystallinity percentage index was estimated using Eq. 2 (Table 7):

$$\% \text{Crystalinity} = \left(\frac{\text{Crystalline Area}}{\text{Total Area}} \right) \times 100. \qquad (2)$$

Mechanical characterization

Digital image correlation (DIC) was used to minimize strain measurement errors during tensile testing (non-contact strain reading) and to have a global perspective of the strain distribution within the tensile sample. The latter provided a check for macroscopic homogeneity of the sample, to confirm the testing which corresponds to pure uniaxial tension. The samples were first painted white by a normal spray and then black dots were put on them by a pneumatic painter. Uniaxial tensile test was performed on a Universal Material Tester (CETR, USA) at a speed of 0.01 mm per second. A 5-mega pixel camera with strain measurement resolution of 25 microstrains was used to capture the strain field during the test. The scale used for correlation was 2.8 μm per pixel. The displacement field was differentiated to obtain the Green–Lagrange strains. Figure 6a shows DIC setup synchronized with the tensile testing machine. Figure 6b shows painted ASTM-638 tensile sample fixed onto the UMT machine.

Results and discussion

Effect of particle size on melting behavior of composite

In order to systematically investigate the effect of particle size on the melting behavior of MA-g-PP composites, the DSC heating scans were obtained after cooling under controlled conditions. Figure 7 shows DSC thermograms of MA-g-PP/silica composites and neat MA-g-PP matrix. In all the samples, a change in the endothermic transition peak was observed due to different melting behaviors of composite materials, which may be because of the formation of different crystal structures during cooling. The heating scans are characterized by observing the endothermic peak temperature (T_m), onset of melting temperature (T_{om}) and heat of fusion (ΔH_f) calculated from the area under the endothermic transition. The results of heating scans are summarized in Table 4. There is no change in the starting (at a much lower temperature) and ending of melting endothermogram. There was a marginal increase in the onset of melting temperature of MA-g-PP by introducing the particles in it to form the composite. Further samples with smaller particle size had higher onset temperature. The endothermic peak temperature was highest for MS 100 nm indicating possession of higher crystallinity

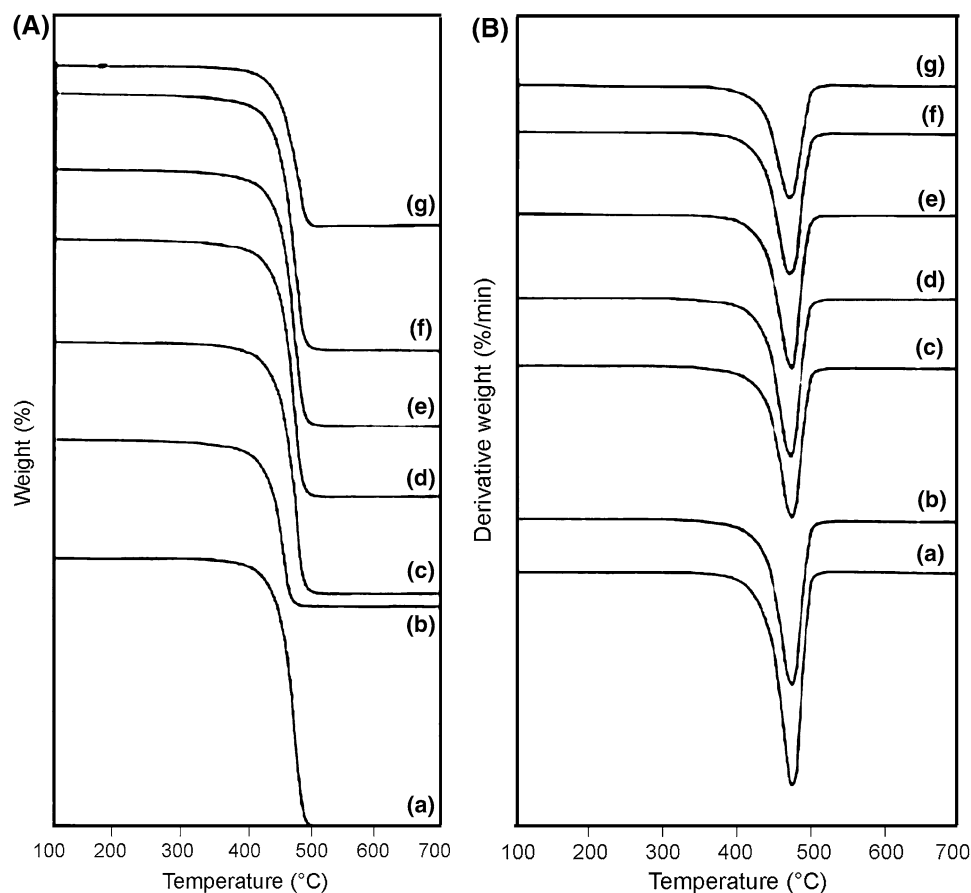**Fig. 4** **a** TGA and **b** DTG thermographs of the composite samples

Table 4 Thermal degradation parameters determined by TGA of the MA-*g*-PP/silica composite

Material	Char yield (%)	Step inflection point (°C)	End temperature (°C)	Onset temperature (°C)
MA-*g*-PP	0.182	440.28	488.55	410.23
MS 130μm	3.80	442.89	456.15	430.31
MS 70μm	3.90	468.75	485.71	432.08
MS 4μm	4.24	469.03	482.39	438.37
MS 750 nm	4.41	471.42	484.94	442.7
MS 250 nm	4.75	472.42	485.86	443.96
MS 100 nm	4.97	473.95	485.18	444.53

followed by MS 250 nm composites. Further, the endothermic peak temperature was reduced in the smaller particle size sample as compared to the larger particle samples. This was clearly observed when the composites sample was subjected to a programmed cooling process which led to the formation of bigger size crystals resulting in the broadness of endothermic peak. The broad fusion range observed in the DSC thermograms presents a wide distribution of crystallite sizes of the MA-*g*-PP.

Effect of filler size on crystallization behavior

A typical DSC cooling scan showing the exothermic transition and the observed characteristic temperatures are shown in Fig. 8. The exothermic transition was characterized by virtue of the following characteristics; the quantity (S_i) is a slope of the initial arm (arbitrary units), (T_s) is an extrapolated onset of exotherm, (T_{c2}) is temperature of start of exotherm, (T_{exo}) is temperature of crystallization, (T_{c1}) is the temperature of completion of exotherm, and (T_s-T_{exo}) is a measure of the overall rate of crystallization.

It was observed that the onset of exotherm (T_s) takes place at higher temperatures in presence of the filler, indicating a faster crystallization process. The various quantities as evaluated from the crystallization exotherms of these samples (Fig. 9) are given in Table 2. There was a 5 °C increase in the exothermic peaks of MA-*g*-PP to MS 100 nm composite samples.

As the particle size decreased in the composite, (T_s-T_{exo}) increased, indicating increase in overall rate of crystallization which corroborates the work of Modesti et al. [31] in the samples with smaller particle size. The higher (S_i) value indicated the higher rate of nucleation.

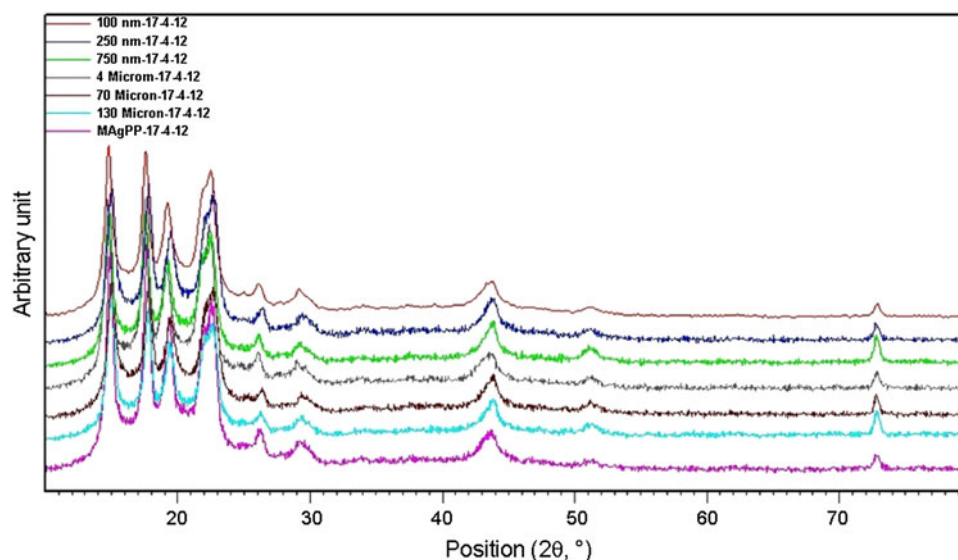**Fig. 5** XRD diffractograms of MA-g-PP/silica composites of different particle sizes

Table 5 D spacing at different peaks from the XRD graphs

Material	D spacing at different peaks								
	∼15°	∼17.5°	∼19°	∼22.5°	∼26°	∼29°	∼44°	∼51°	∼73°
MA-g-PP	5.97	5.01	4.5921	3.922	3.40	3.0566	2.068	1.78	1.296
MS 130μ	5.917	5.018	4.562	3.909	3.396	3.049	2.066	1.7848	1.297
MS 70μ	5.90	5	4.56	3.9	3.38	3.041	2.076	1.785	1.297
MS 4μ	6	5.09	4.63	3.95	3.42	3.07	2.071	1.785	1.297
MS 750 nm	5.98	5.05	4.6	3.93	3.41	3.06	2.06	1.785	1.297
MS 250 nm	5.9	5.001	4.563	3.90	3.38	3.03	2.076	1.785	1.297
MS 100 nm	6	5.06	4.59	3.93	3.416	3.06	2.071	1.787	1.297

Table 6 Intensity of the peaks obtained from the XRD graph

Material	Peak intensity at different angles									Total intensity
	∼15	∼17.5	∼19	∼22.5	∼26	∼29	∼44	∼51	∼73	
MA-g-PP	2,382.3	2,147	1,617.6	1,882.3	588.2	529.4	764.7	441.1	588	10,940.6
MS 130μ	2,550.9	2,423.5	1,676.4	2,117.6	717.5	658.7	852.94	470.5	529.32	11,997.36
MS 70μ	2,551.3	2,454.3	1,702.7	2,189	702	621.6	810	497	500	12,027.9
MS 4μ	2,600	2,558.8	1,774.7	2,418.2	705.8	658.8	852.9	529.4	647	12,745.6
MS 750 nm	2,623.5	2,664.7	1,798.3	2,590	764.6	705.8	794	511	480.4	12,932.3
MS 250 nm	2,729.4	2,670.5	1,805.8	2,647	794.1	647.05	764.7	441.17	499.9	12,999.62
MS 100 nm	2,731.6	2,647.5	1,861.9	2,635.8	778.4	623.7	786.9	431	501.2	12,998

The quantity (S_i) increased with decrease in the particle size indicating an increase in the rate of nucleation.

A high rate of nucleation might have caused the formation of a large number of spherulites, which could not grow to a large size due to a high rate of crystallization (higher cooling rate). Thus, the samples with small particles contained a large number of small spherulites.
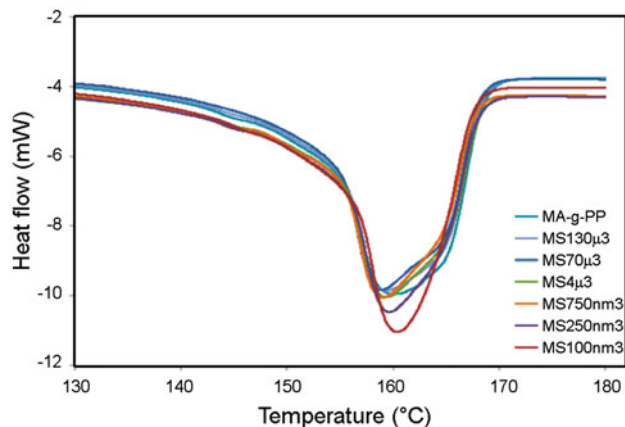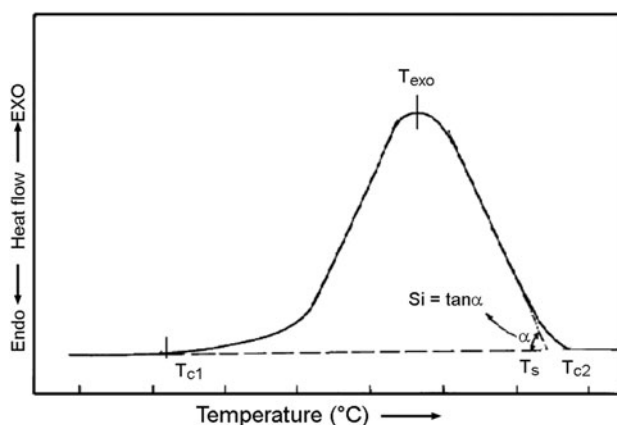
TGA

From Fig. 4, it can be observed that the degradation of MA-g-PP/silica composites is a single stage process in the temperature range of 350–500 °C, it is because of good thermal stability of polypropylene and silica constituents of the composites. The thermal degradation mechanism

Table 7 X_c (%) obtained from XRD

Material	X_c (%)
MA-g-PP	47.9431544
MS 130μ	60.2947159
MS 70μ	60.8594411
MS 4μ	60.958925
MS 750 nm	62.5902353
MS 250 nm	66.7220233
MS 100 nm	66.2547159

Fig. 7 DSC thermograms showing the effect of filler size on melting behavior

may involve a random chain scission at the weak links along the polymer backbone that produces large amounts of hydrocarbon products. The degradation depends on the particle encapsulation and extent of interaction with matrix as described by Kumar et al. [32] for fiber composites. Enhanced thermal stability is commonly observed when filler particles are well-dispersed into the polymer matrix, as a result of hindered out-diffusion of the volatile decomposition product and also of carbonaceous-silicate char formation that acts as a physical barrier effect of filler that hinders the diffusion of heat and degradation of volatiles from the bulk [10, 11]. The thermal stability of various composite formulations can be compared by onset temperature shown in Table 4. The higher value of onset temperature was an indication of the higher stability of composites, which resulted in improvement in the thermal stability of MA-g-PP by addition of the silica particles. Further, the thermal stability increased when moving from MS 130 μm down to MS 100 nm. This single step degradation was confirmed by the observed single peak in the

Fig. 8 Typical DSC thermograms showing the exothermic transition and characteristic temperatures
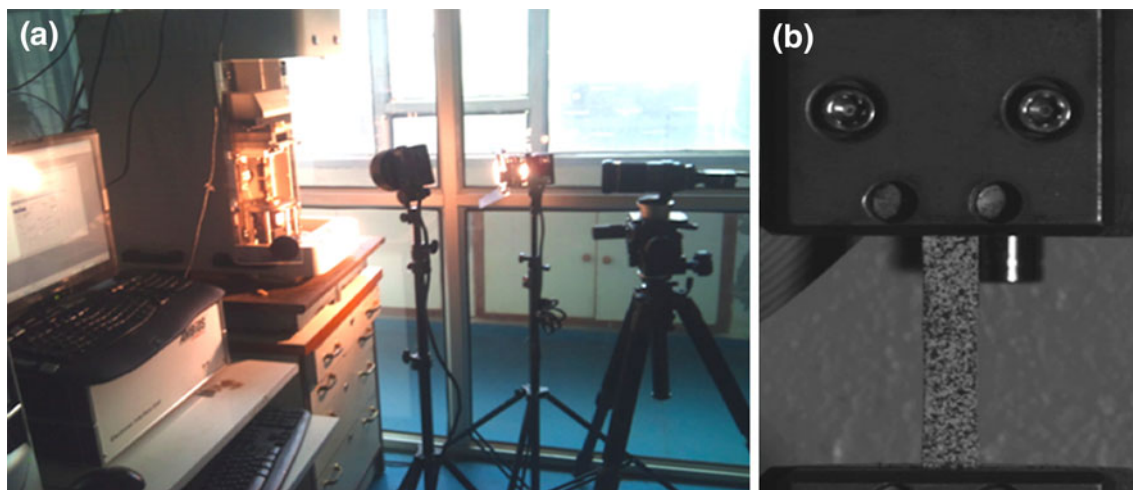
Fig. 6 a DIC setup synchronized with the tensile testing machine and **b** painted tensile sample fixed onto the UMT grips
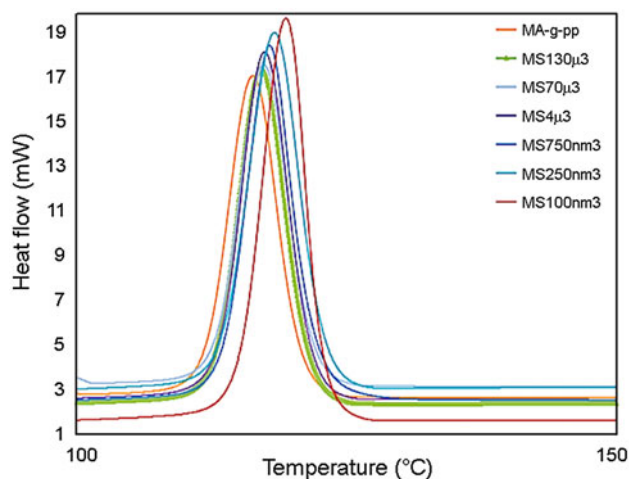
Fig. 9 DSC thermograms of composites with different particle sizes showing the exothermic transition

Fig. 10 Young's modulus of composite samples of different particle sizes

DTG traces. The char yield increased from 0.182 % in MA-*g*-PP to 4.97 % in a MS 100 nm sample due to increased interactions between the filler with the matrix which were the result of larger surface area of smaller silica particles.

X-ray diffraction

The X-ray diffractograms of MA-*g*-PP and its composites are shown in Fig. 5. The peaks existed at about 9 angles. The X-ray peak that appeared in the matrix was also observed in the composites. The overall peak intensity as compared to neat MA-*g*-PP was increased due to increase in the trans-crystallinity as shown in Table 6. The peak intensity is directly dependent on the distribution of particular atoms in the structure and increase in peak intensity suggests the structural perfection as Rousseaux et al. [30].

There was a slight increase in the peak intensity moving from MS 130 µm down to MS 250 nm. The higher peak intensity indicated higher crystallization of melt during cooling.

The relative decrease in intensity of peak in the MS 100 nm as compared to MS 250 nm could be due to slight agglomeration of silica particles in MS 100 nm sample which resulted in smaller crystalline area or it could be due to the fact that the samples with small particles contained a large number of small spherulites that were responsible for the decrease in the overall crystallinity.

The values of the D spacing remained constant and dependent only on the shape of unit cell, which did not change on the addition of filler. The peak positions are indicative of the crystal structure.
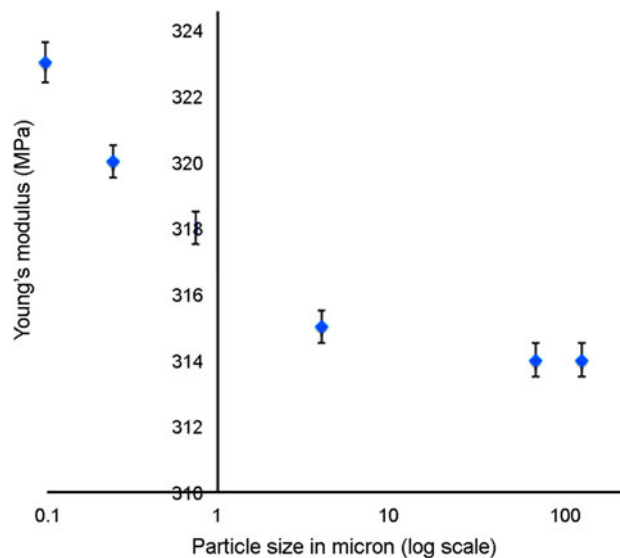
Young's modulus

It has been mentioned in the literature that the change in size of micron-scale particles does not have significant influence on the composite modulus [25, 28, 29], whereas in this study Young's modulus of polymeric matrix (MA-*g*-PP) increases by adding 130 µm particles by 18 %. From Fig. 10, it can be observed that the Young's modulus of the composite samples further increases slightly with reduction of particle size from 130 µm to 100 nm.

Ultimate strength

The ultimate strength strongly depends on the stress transfer between the particles and the matrix. For well-bonded particles, the applied stress can be effectively transferred to the particles from the matrix [33]. Strength of MA-*g*-PP being 30 MPa does not improve by adding particles larger than 1 micron samples (Fig. 11). The improvement can be seen in composite samples containing particles of sizes less than 1 µm. The increase may be attributed to hydrogen bonding between the free hydroxyl groups present on the silica particle's surface and MA of the matrix while the neutral effect in sizes above 1 µm samples could be due to lack of free hydroxyl groups on its surface as compared to smaller size particles. This proved that there was a good interaction between the matrix and the particles of less than 1 µm composite samples. Strength increases with the increasing surface area of the filled particles through a more efficient stress transfer mechanism. It is for this reason that smaller particles having higher total surface area for a given particle loading have higher value of strength.
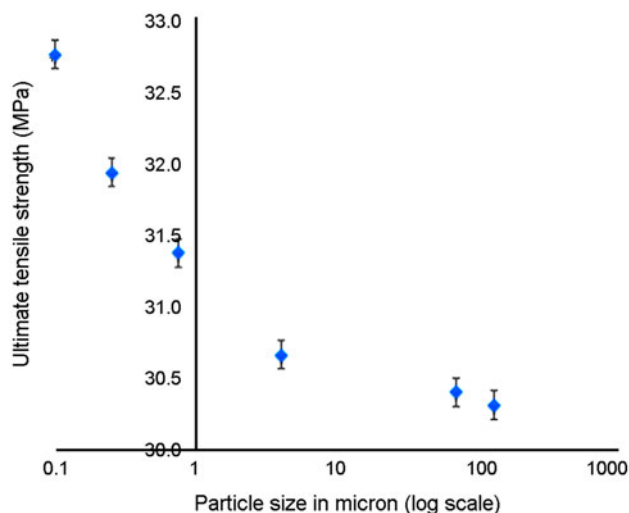
Fig. 11 Ultimate tensile strength of composite samples of different particle sizes

Conclusion

- Composite samples of smaller particle size had a higher value of S_i (tanα) indicating higher overall rate of crystallization.

- The results revealed that melting endotherm is comparatively unaffected by addition of dispersed phase although a marginal increase in the melting onset temperature was noticed for composites containing smaller particle size of silica.

- The thermal stability of matrix was increased by incorporation of silica spheres. Further increase in thermal stability was observed for smaller reinforcement size.

- The increasing trend of crystallinity of composite material was observed for reduced size of dispersed phase. The lowest crystallinity percentage, observed from WAXD diffractograms, was seen for neat MA-g-PP followed by 130 micron silica particle whereas the highest value of crystallinity was obtained for a matrix reinforced with 100 nm silica particles.

- The Young's modulus was found to be increasing with the addition of the silica spherical particles and further increases for the composites containing larger particle size. This can be understood in the light of the fact that dispersed silica phase is much stiffer than the thermoplastic counterpart. The modulus being a stiffness parameter which governs by the size and amount of dispersed phase whereas the strength depends upon the size and shape of crystallites. It was also observed that strength increases with reduction in particle size. This is an indirect confirmation of the fact that smaller particle size of dispersed phase leads to large number of crystallites of smaller dimensions that provides better

transmission of internal stresses throughout the matrix which exhibits higher strength-at-break.

References

1. Juhasz JA, Best SM, Brooks R, Kawashita M, Miyata N, Kokubo T, Nakamura T, Bonfield W (2004) Mechanical properties of glass-ceramic A-W-polyethylene composites: effect of filler content and particle size. Biomaterials 25:949–955

2. Cho J, Joshi MS, Sun CT (2006) Effect of inclusion size on mechanical properties of polymeric composites with micro and nano particles. Compos Sci Technol 66:1941–1952

3. Mishra S, Sonawane SH, Singh RP (2005) Studies on characterization of nano CaCO₃ prepared by the in situ deposition technique and its application in PP–nano CaCO₃ composites. J Polym Sci Part B Polym Phys 43:107–113

4. Nakamura Y, Yamaguchi M, Okubo M, Matsumoto T (1992) Effects of particle size on mechanical and impact properties of epoxy resin filled with spherical silica. J Appl Polym Sci 45: 1281–1289

5. Reynaud E, Jouen T, Gauthier C, Vigier G, Varlet J (2001) Nano fillers in polymeric matrix: a study on silica reinforced PA6. Polymer 42:8759–8768

6. Wu GH, Chen GQ, Zhu DZ, Zhang Q, Jiang LT (2005) Effect of particle size on thermo-physical properties of SiCp/Cu composites fabricated by squeeze casting. Trans Nonferrous Met Soc China 15:217–220

7. Shiratori Y, Magrez A, Pithan Ch (2005) Particle size effect on the crystal structure symmetry of K₀.₅Na₀.₅NbO₃. J Eur Ceram Soc 25:2075–2079

8. Sreekanth MS, Bambole Mhaske ST, Mahanwar PA (2009) Effect of concentration of mica on properties of polyester thermoplastic elastomer composites. J Mineral Mater Charact Eng 8:271–282

9. Ha SR, Ryu SH, Park SJ, Rhee KY (2007) Effect of clay surface modification and concentration on the tensile performance of clay/epoxy nanocomposites. Mater Sci Eng A 448:264–268

10. Chang TE, Kisliuk A, Rhodes SM, Brittain WJ, Sokolov AP (2006) Conductivity and mechanical properties of well-dispersed single-wall carbon nanotube/polystyrene composite. Polymer 47:7740–7746

11. Wetzel B, Haupert F, Zhang MQ (2003) Epoxy nanocomposites with high mechanical and tribological performance. Compos Sci Technol 63:2055–2067

12. Goyanes SN, Konig PG, Marconi JD (2003) Dynamic mechanical analysis of particulate-filled epoxy resin. J Appl Polym Sci 88: 883–892

13. Park SJ, Jin FL, Lee C (2005) Preparation and physical properties of hollow glass microspheres-reinforced epoxy matrix resins. Mater Sci Eng A 402:335–340

14. Goyal RK, Tiwari AN, Mulik UP, Negi YS (2007) Effect of aluminum nitride on thermomechanical properties of high performance PEEK. Compos Part A Appl Sci Manuf 38:516–524

15. Hu YH, Chen CY, Wang CC (2004) Viscoelastic properties and thermal degradation kinetics of silica/PMMA nanocomposites. Polym Degrad Stab 84:545–553

16. Zhou YX, Pervin F, Rangari VK, Jeelani S (2006) Fabrication and evaluation of carbon nano fiber filled carbon/epoxy composite. Mater Sci Eng A 426:221–228

17. Basara G, Yilmazer U, Bayram G (2005) Synthesis and characterization of epoxy based nanocomposites. J Appl Polym Sci 98:1081–1086

18. Ash BJ, Siegel RW, Schadler LS (2005) Glass-transition temperature behavior of alumina/PMMA nanocomposites. J Polym Sci Part B Polym Phys 42:4371–4383

19. Preghenella M, Pegoretti A, Migliaresi C (2005) Thermo-mechanical characterization of fumed silica-epoxy nanocomposites. Polymer 46:12065–12072

20. Huang YQ, Jiang SL, Wu LB, Hua YQ (2004) Characterization of LLDPE/nano-SiO$_2$ composites by solid-state dynamic mechanical spectroscopy. Polym Test 23:9–15

21. Sandler J, Werner P, Shaffer MS, Demchuk V (2002) Carbon-nanofibre-reinforced poly(ether ether ketone) composites. Compos Part A Appl Sci Manuf 33:1033–1039

22. Bragato G, Gianotti G (1983) High speed spinning of poly(ethylene terephthalate)—II: orientation induced mechanism of cold crystallization in pre-orientated yarns. Eur Polym J 19:803–809

23. Ajayan PM, Schadler LS, Braun PV (2003) Nanocomposite science and technology. Wiley, New York, ISBN: 3527303596

24. Kamigaito O (1994) What can be improved by nanometer composites? J Jpn Soc Powder Metall 38:315–321

25. Dekkers MEJ, Heikens D (1983) The effect of interfacial adhesion on the tensile behavior of polystyrene–glass-bead composites. J Appl Polym Sci 28:3809–3815

26. Fu SY, Lauke B (1998) Characterization of tensile behavior of hybrid short glass fiber calcite particle ABS composites. Compos A 29:575–583

27. Radford KC (1971) The mechanical properties of an epoxy resin with a second phase dispersion. J Mater Sci 6:1286–1291

28. Lau KT, Gu C, Hui D (2006) A critical review on nanotube and nanotube/nanoclay related polymer composite materials. Compos B 37:425–436

29. Yang J, Sang Y, Chen F, Fei Z, Zhong M (2012) Synthesis of silica particles grafted with poly ionic liquid and their nucleation effect on microcellular foaming of polystyrene using supercritical carbon dioxide. J Supercrit Fluids 62:197–203

30. Rousseaux DJ, Sclavons M, Godard P, Marchand-Brynaert J (2012) Tuning the functionalization chemistry of polypropylene for polypropylene/clay nanocomposites. React Funct Polym 72:17–24

31. Modesti M, Lorenzetti A, Bon D, Besco S (2006) Thermal behaviour of compatibilised polypropylene nanocomposite: effect of processing conditions. Polym Degrad Stab 91:672–680

32. Kumar S, Choudhary V, Kumar R (2010) Study on compatibility of unbleached and bleached bamboo fiber with LLDPE matrix. J Therm Anal Calorim 102:751–761

33. Hsueh CH (1987) Effects of aspect ratios of ellipsoidal inclusions on elastic stress transfer of ceramic composites. J Am Ceram Soc 72:344–347